This is a post-peer-review, pre-copyedit version of an article published in Journal of Archaeological Science: Reports. The final authenticated version is available online at: https://doi.org/10.1016/j.jasrep.2018.02.030

The Misérègne slag deposit (Valle d'Aosta, Western Alps, Italy): insights into (pre-)Roman copper metallurgy

Luca Toffolo (1), Anna Addis (1), Silvana Martin (1), Paolo Nimis (1), Mauro Rottoli (2), Gaston Godard (3)

(1) Geosciences Department, University of Padua, via G. Gradenigo 6, 35131 Padua, Italy

(2) ARCO Cooperativa di Ricerche Archeobiologiche, via Crispi 12, 22100 Como, Italy

(3) Institut de Physique du Globe de Paris, Université Paris-Diderot, UMR 7154 CNRS, F-75252 Paris Cedex 05, France

ABSTRACT

The Misérègne hamlet (Fénis village, Valle d'Aosta region, Italy) rises on a huge metallurgical slag deposit, whose origin has so far been unknown. Here we provide the first detailed textural, mineralogical and chemical characterization of the slags and the results of radiocarbon dating of charcoal fragments contained therein. Three types of slags are found, i.e., coarse, massive and flat, which are composed of olivine, spinel and pyroxene crystals in a glassy matrix rich in anorthite ± magnetite/ulvöspinel crystallites. All the slags contain matte droplets, which show a Cu-enrichment from the coarse and the massive slags (intermediate solid solution, ~$CuFeS_2$, or bornite solid solution, ~Cu_5FeS_4 + abundant pyrrhotite solid solution, ~$Fe_{1-x}S$) to the flat slags (bornite only). Olivine morphology indicates slow cooling for the massive slags (mostly euhedral crystals), rapid cooling for the coarse slags (dendritic crystals) and slow cooling followed by quenching, consistent with tapping, for the flat slags (euhedral-dendritic transitional crystals). Bulk slag compositions and olivine-spinel

geothermometry suggest that the coarse and massive slags are genetically related (T = 880−1090 °C and T = 860−1140 °C for coarse and massive slags, respectively), while the flat slags are distinct higher-temperature melts (T = 1020−1415 °C). The data suggest a multiple-step smelting process, by which an impure chalcopyrite ore, was first smelted to produce relatively Cu-poor matte and coarse and massive slags; the matte was then reprocessed at higher temperature to produce more copper metal and flat slags. Based on radiocarbon dating, the Misérègne slags date back to the II-I century BCE and thus constitute the earliest known record of metallurgical activity in the north-western Italian Alps.

1. INTRODUCTION

The Valle d'Aosta region (Western Alps, north-eastern Italy) has been an important mining and metallurgical center until the second half of the XX century, as testified by numerous mines and metallurgical sites (Castello, 1981; Nicco, 1987). Written records for metallurgical activity in the region are very scarce before the XIX century (Nicco, 1987), even though the presence of a medieval activity was demonstrated by dating of charcoal in slags from the Servette copper mine (Tumiati et al., 2005). In this work, we present new radiocarbon dating from the Misérègne slag deposit (Fénis), yielding the first evidence of (Pre-)Roman metallurgical activity in the region, whose existence had previously been only hypothetical (Robilant, 1786, 1788). We also characterize the Misérègne slags following an established petrologic approach (Bachmann, 1982; Sáez et al., 2003; Tumiati et al., 2005; Addis et al., 2016), in combination with geothermometric techniques (olivine-spinel geothermometry), in order to obtain technological information and precise estimates of furnace working temperatures.

1.1. The Misérègne site

Misérègne is the easternmost hamlet of the Fénis village and is located on the apex of the alluvial fan of the Clavalité torrent, in the valley floor of the southern Valle d'Aosta (Fig. 1a). This portion of the valley is literally cluttered with mines and prospects (Fig. 2) where iron and iron-copper ores were exploited. The Fe ores are composed of dominant magnetite and are hosted in serpentinites (e.g., Lac Gelé, Ponton, Ussel mines); the Fe-Cu ores typically consist of pyrite and chalcopyrite in variable proportions, together with accessory magnetite, sphalerite, pyrrhotite and bornite. They are found as massive, semi-massive and disseminated concentrations hosted in chlorite schists (chlorite + minor garnet, quartz, talc, chloritoid and sodic amphibole), talc schists (talc + minor glaucophane, garnet, chloritoid, clinozoisite/epidote, paragonite, talc), glaucophanites (glaucophane + minor garnet, chloritoid, clinozoisite/epidote, paragonite, talc) and quartzites (quartz + minor garnet) (Castello 1981; Martin et al., 2008). All these lithologies belong to the same geological unit, i.e., the ophiolitic Piemonte Zone (Martin et al. 2004 and ref. therein).

Misérègne rises on a huge metallurgical slag deposit, which is called *Ferrùn* (i.e., slag; Gerbore, 2000) by the inhabitants. The site was referred to with the same name in a document dating to 1332 (Di Gangi, 1999), but no mention of the origin of the deposit was made. The slag deposit is composed of two parts (Fig. 1a): the first is an exposed slag heap (N 45°44'02", E 7°30'31"), 4200 m^2-area and 6 m thick (at least); the other is a buried deposit (N 45°43'59" E 7°30'33"), which underlies the village and whose extension is hardly computable because of the urbanization of the area. The former is probably a dump produced in recent times, in which slags and modern inert waste are mixed together. The latter was fortuitously exposed in 2011 during the excavation for the foundations of a house and seems to be pristine.

2. MATERIAL, INSTRUMENTATION AND METHODOLOGIES

Seventeen slag specimens were sampled from the buried slag deposit (see Supplementary material). Six of them, i.e., two specimens representative for each slag type (see details below), were analyzed.

81 The samples were prepared in thin (30-μm thick) polished sections and studied with an optical
82 microscope under transmitted and reflected polarized light and with a scanning electron microscope
83 (SEM). We used a Nikon Eclipse ME 600 optical microscope and a CamScan MX 2500 SEM
84 (Geosciences Department, University of Padua, Italy) equipped with a LaB_6 crystal and an energy-
85 dispersive spectrometer (EDS), working at 20-kV accelerating voltage and 40 nA current.
86 The quantities of crystalline and amorphous phases of the bulk samples were estimated from X-ray
87 powder diffraction (XRPD) data. XRPD data were collected using a Bragg–Brentano θ-θ
88 diffractometer (PANalytical X'Pert PRO, Cu Kα or Co Kα radiation, 40 kV and 40 mA) equipped
89 with a PiXcel detector. Ten wt% ZnO was used as internal standard. Diffraction patterns were
90 interpreted using the X'Pert HighScore Plus 3.0 software by PANalytical, qualitatively reconstructing
91 mineral profiles of the compounds by comparison with the powder diffraction files from the
92 International Centre for Diffraction Data. Then, mineralogical quantitative phase analyses were
93 performed using the full-profile method (Rietveld, 1969). Refinements were accomplished with the
94 TOPAS software (v.4.1) by Bruker AXS.
95 Microchemical analyses (volume of ~1 μm^3) were performed at the Department of Earth Sciences of
96 the University of Milan (Italy), using a JEOL JXA-8200 electron probe micro-analyzer (EPMA)
97 equipped with five wavelength-dispersive spectrometers (WDS) and one EDS. Twelve elements were
98 analyzed by WDS spectrometry using these standards: olivine (Mg), omphacite (Na), galena (S),
99 rhodonite (Mn), K-feldspar (K), almandine garnet (Al, Fe), wollastonite (Si), anorthite (Ca), pure Cr,
100 nickeline (Ni), pure Cu, and ilmenite (Ti). Working conditions were a 15-kV accelerating voltage,
101 with a 5-nA beam current intensity, and counting times of 30 s for the peak and of 10 s for the
102 background. Detection limits were (in μg/g or ppm): Al: ~180; Ca: ~150; ~Cr: 260; Cu: 540; Fe: ~390;
103 K: ~120; Mg: ~180; Mn: ~360; Na: ~180; Ni: ~440; S: ~260; Si: ~200; Ti: ~330.
104 Bulk chemical compositions were measured at the Geosciences Department of the University of Padua
105 by X-ray fluorescence (XRF) spectrometry, using a Philips PW2400 (XRF) wavelength-dispersive
106 sequential spectrometer equipped with a Rh tube. Reference standards were natural geological

samples (Govindaraju, 1994). The relative analytical precision is estimated to be within ±0.6% for major and minor elements and within ± 3% for trace elements. Samples were prepared as fine powder (<10 μm grain size) using Retsch M0 mortar grinder and Retsch RS100 vibratory disk mill. Large quantities of powder (about 100 g for each sample) have been prepared for the coarse slags, because of their heterogeneity. The high Fe and S contents of the slags hindered the production of fused beads; therefore, powder samples were pressed into 3 g pellets. The quantitative analyses were performed using the SuperQ software package.

FeO was determined by potassium permanganate titration (permanganometry; see Appendix for the details of the method).

Furnace working temperatures were estimated using an olivine-spinel geothermometer, which is based on equilibrium Fe^{2+}–Mg partitioning between olivine and spinel (Irvine, 1965; Sack and Ghiorso, 1991). Among existing versions of this geothermometer, we have chosen that of Sack and Ghiorso (1991) because is calibrated in the temperature range 400-1400°C, and thus ~~should~~ include the typical working temperatures of ancient furnaces (Bachmann, 1982; Tylecote, 1992), and can be applied down to atmospheric pressure (~0.1 MPa). To avoid possible disequilibrium issues, the olivine-spinel geothermometer was generally applied on crystals in apparent textural equilibrium, i.e., small (10−20 μm in diameter) polyhedral hercynites included in euhedral olivines. In addition, we only chose hercynites that were sitting near the Mg-rich (i.e., high-temperature) cores of the olivines, which are supposed to represent "frozen" high-temperature assemblages. Olivine and spinel compositions were measured by EPMA, focusing the electron beam a few microns away from the hercynite-olivine crystal boundary in order to avoid mixed analyses. In the coarse slags, spinel inclusions in euhedral olivines were too small to be analyzed without appreciable contamination by the host olivine. Therefore, the analyses were performed on polyhedral hercynite included in the cores of big skeletal olivine crystals, choosing only olivines free of glass inclusions near their cores.

Charcoal fragments contained in the slags were dated using the ^{14}C technique. We selected five slag samples from different stratigraphic levels in the buried deposit, i.e., two coarse slags (FE-G10, FE-

G11) from the uppermost (0.4−1.0 m) level and two coarse and one massive slag (FE-G12, FE-G13, FE-G3) from the lowermost (1−3 m) level (see details in Table 3). Whenever possible, we sampled fragments derived from thin tree branches, which belonged to the youngest parts of the tree and whose ages are thus, presumably, closer to that of the slag. Radiocarbon dating was performed at the Poznan Radiocarbon Laboratories (Poznan, Poland) and at the CEDAD laboratories (Brindisi, Italy) of the University of Salento (Lecce, Italy), using an accelerator mass spectrometer, following a standard procedure [see instrumental and methodological details at http://radiocarbon.pl/index.php?option=com_frontpage&Itemid=1 (Poznan) and in Calcagnile et al., 2004, D'Elia et al., 2004 (CEDAD)].

3. RESULTS

3.1. The buried deposit of Misérègne and macroscopic features of the slags

As revealed by our survey in 2011, the buried slag deposit of Misérègne is a lenticular body with a convex upper surface and a maximum observed thickness of 3.4 m, thinning northwards and westwards and extending southwards beneath the village (Fig. 1a, b; Fig. 3). The base is flat and lies on proximal alluvial fan sediments. In the studied section, the slag deposit is covered by soil and is characterized by an open texture, with scarce sandy matrix. Its upper portion shows an E-dipping cross-stratification. Based on the digital terrain model, we estimate the volume of the deposit to be > 60000 m^3 (assuming an area of ~22000 m^2 and an average thickness of 3 m).

The slags are typically fragments with a mean size of 2−5 cm; 10−20 cm pieces are not frequent and those measuring more than 20 cm are rare and tend to crumble easily. The slags are dark grey, with brown coatings due to alteration to iron oxides/hydroxides (e.g. goethite, $Fe^{3+}O(OH)$). Slags are frequently stained by green-blue minerals, which probably consist of copper sulfates, carbonates and

159 silicates. Frequently, mm-to-cm-sized pieces of partly carbonized wood or charcoal protrude from
160 the surfaces of the slag or are included in them. Fragments of quartz and chlorite schist are other
161 common macroscopic inclusions.
162 Based on their morphology and on a qualitative estimate of porosity, we grouped the slags into three
163 categories, as suggested by Addis et al. (2016):

164 - *Coarse* slags (samples FE-G10, FE-G11, FE-G12), which have a lumpy and angular
165 morphology and exhibit the highest degree of porosity (Fig. 4a). Charcoal fragments can be
166 abundant both on the surface or as inclusions. Coarse slags can trap on their surfaces sand- to
167 gravel-sized quartz grains and lithic fragments (chlorite schist and talc schist).
168 - *Massive* slags (samples FE-G3, FE-C1), which have smooth or broken surfaces and very low
169 porosity (Fig. 4b). They are dense, and hard to crush and resemble an aphanitic volcanic rock
170 (e.g., a basalt). Charcoal fragments are rare and superficial.
171 - *Flat* slags (samples FE-P5, FE-P6), which have a maximum thickness of ca. 2 centimeters and
172 a low porosity (Fig. 4c, d). They have two main surfaces: one irregular, typically including
173 sand-sized rock fragments, and the other smooth or corrugated with "ropes" that indicate the
174 sense of the flow. Charcoal pieces are uncommon and superficial.

175 In addition, large (up to ~30 cm) composite slag blocks occur, which show a lumpy upper surface
176 and a lower surface composed of welded angular fragments (up to a few centimeters) of all major
177 slag types.
178
179 3.2. Microscopic description
180
181 All the slags are composed ~~by~~ of a dominant silicate fraction, i.e., the slag *stricto sensu*, comprising
182 variable proportions of crystals and glass, and ~~by~~ of a mixture of sulfides, i.e., the matte.
183
184 *3.2.1. The silicate slag*

185 In all the slags, the most abundant and largest crystals are those of olivine [forsterite (Fo: Mg_2SiO_4)-
186 fayalite (Fa: Fe_2SiO_4) solid solution] and spinel-group minerals [solid solutions of hercynite
187 ($FeAl_2O_4$), spinel ($MgAl_2O_4$), magnetite (Fe_3O_4), and ulvöspinel (Fe_2TiO_4), endmembers]. The
188 compositions of slag minerals are reported in Supplementary material.
189 Olivine. It always shows a concentric compositional zoning, which reflects the progressive rimward
190 increase in fayalite (Fe_2SiO_4) component. Olivine crystals in the three classes of slags have different
191 compositions and morphologies. In the *coarse* slags (Fig 5a), olivine (Fo_{52-34}; ~29−34 wt%; Table 1)
192 mainly forms dendritic crystals, which surround a few large (up to 1.5 mm) skeletal olivine grains;
193 polyhedral (i.e., euhedral) olivines are rare and are usually found as aggregates of small (up to 50
194 μm) crystals. In the *massive* slags (Fig 5b), most of the olivine crystals (Fo_{53-18}; ~35−45 wt%; Table
195 1) are large (100−200 μm) and polyhedral, but some of them are transitional to the skeletal type.
196 Dendritic crystals are infrequent, but they can be locally abundant. In the *flat* slags (Fig 5c), olivine
197 (Fo_{56-21}; ~47−60 wt%; Table 1) mostly forms chain-like dendritic crystals near the smoother surface
198 and little (≤100 μm) polyhedral crystals that progressively become more abundant towards the more
199 irregular surface; some crystals exhibit polyhedral to dendritic transitional shapes.
200 Spinel-group minerals. They are mainly represented by a spinel-hercynite solid solution, in which the
201 hercynitic component is predominant. In all slag types (Fig 5a, b, c), hercynite crystals are always
202 polyhedral, with dimensions ranging from a few μm to 100 μm, and are frequently included in olivine.
203 Hercynite inclusions are unzoned, but crystals that are dispersed in the matrix may exhibit a thin (<3
204 μm) Fe-enriched rim. The late generation minerals consist of skeletal crystals either of ulvöspinel
205 (actually a $Fe^{2+}_2TiO_4$-$Fe^{2+}Al_2O_4$ solid solution, with prevailing Ti-bearing endmember) in the massive
206 slags, or of Ti-bearing magnetite in the flat slags. In the flat slags, moreover, the smooth or corrugated
207 surface is lined by a thin (~10 μm) layer of skeletal magnetite crystals.

208 Orthopyroxenes. A Mg-Al-rich ferrosilite ($Fe_{0.97}Mg_{0.80}Al_{0.37}Ti_{0.03}Si_{1.79}O_6$) was found in the coarse
209 slags, forming long (up to several 100 μm) skeletal to dendritic crystals around quartz and talc relicts.
210 In the other slag types, ferrosilite has been identified only by XRPD.
211 Matrix. In all slag types, the groundmass surrounding olivine and hercynite crystals is a mixture of
212 crystallites and of Si-Al-Fe-Ca-Ti glass. The highest proportion of glass is observed in the coarse
213 slags (~49−51 wt%; Table 1), while in the massive and flat slags the groundmasses are crystallite-
214 rich. Based on XRPD data, the crystallites are probably composed of hedenbergite and anorthite
215 ($CaAl_2Si_2O_8$) minor ilmenite ($FeTiO_3$) and abundant magnetite/ulvöspinel were also observed in the
216 massive slags and in the flat slags, respectively.
217 Relict phases. Millimetric aggregates of anhedral and rounded Fe-oxides associated with metallic
218 copper patches (<50 μm) ± metallic iron are found in both coarse and massive slags (Fig 5d). Coronae
219 of tiny polyhedral crystals of hercynite occur around the aggregates, suggesting a reaction with the
220 molten slag. Relicts of quartz (SiO_2) and talc [$Mg_3Si_4O_{10}(OH)_2$] have also been observed in all slag
221 types, although they are more abundant in coarse and massive slags. In the coarse slags, mm to cm-
222 sized domains with sharp boundaries are frequently found, in which the slag texture appears to be
223 different from the prevailing one: we interpret these domains as fragments of resmelted slags.
224 Alteration phases. Fractures, bubbles and charcoal pores are often filled with iron oxyhydroxides
225 [e.g., goethite, FeO(OH)] and carbonates (calcite, $CaCO_3$, identified by XRPD), derived from the
226 weathering of sulfides in the slags (Fig. 5d) and the percolation of carbonate enriched meteoric fluids.
227
228 *3.2.2. The matte*
229 The matte forms dispersed droplets and irregular patches in the silicate slag. The matte is composed
230 of anhedral and rounded, rarely dendritic, crystals. Three sulfide solid solutions were identified (Fig.
231 6): pyrrhotite (Po_{ss}, ~$Fe_{1-x}S$), bornite (Bn_{ss}, ~Cu_5FeS_4) and 'intermediate solid solution' (*iss*,
232 ~$CuFeS_2$). Frequently, Bn_{ss} and Po_{ss} form symplectitic intergrowths. The size, shape and composition
233 of the sulfides vary across the three types of slags. In the *coarse* slags, sulfides occur as irregular

234 patches, reaching 2−3 mm in size, or as droplets up to 1.3 mm in diameter (Fig 7a, b). Up to 10 μm-
235 sized sulfide droplets are disseminated throughout the slag. Common sulfide associations are Bn_{ss} +
236 Po_{ss} and Po_{ss} + *iss*. Relict chalcopyrite fragments are common (Fig 7c). In the *massive* slags, the
237 sulfides are less abundant (Fig 7d); they ~~and~~ occur as round or elliptical droplets with a diameter of
238 up to 1 cm and as smaller (10−30 μm) disseminated droplets. Sulfide associations and compositions
239 are the same as in the coarse slags. In the *flat* slags, the droplets have a diameter generally lower than
240 10 μm and rarely up to 230 μm (Fig 7e). They have a dominant Bn_{ss} composition and, therefore, a
241 higher mean Cu/Fe ratio than those in the other slag types. In all slag types, Bn_{ss} and *iss* are frequently
242 altered into microgranular digenite (~Cu_9S_5) + covellite (CuS), growing from fractures, grain
243 boundaries and the matte-slag interface (Fig. 7f).
244 Patches of metallic iron and copper were occasionally observed in the matte drops. Iron forms round
245 anhedral grains and is sometimes intergrown with sulfides. Copper is a late phase, which fills voids
246 (pores and fractures) and sometimes forms curls protruding from the matte towards the void space.
247
248 3.3. Slag bulk chemistry
249
250 The XRF bulk chemical compositions of the slags are reported in Table 1 and plotted in the SiO_2-
251 FeO-Al_2O_3 ternary diagram of Levin et al. (1964; Fig. 8). This simplified chemical system can suitably
252 be adopted to describe the slags, since the sum of the three oxides makes up a great part of the slag
253 weight (~76−85 %). The coarse and massive slags have very similar compositions, although the SiO_2
254 concentration in the coarse slag may have been overestimated by a few wt% units because of the
255 presence of unreacted quartz relicts. This notwithstanding, both slag types plot near the 1088°C
256 fayalite-hercynite-Fe-cordierite-melt peritectic point, which is only 5 °C above the fayalite-Fe-
257 cordierite-tridymite-melt eutectic. The flat slags plot close to the fayalite-hercynite cotectic line, since
258 they contain more FeO and less SiO_2. Moreover, the flat slags have lower contents of Cu (~0.6−0.9
259 wt%) than the coarse (~1.2−1.4 wt%) and massive (~1.0−1.3 wt%) slags.

3.4. Geothermometry

The temperature estimates obtained for the olivine-spinel crystal pairs are reported in Table 2. The coarse and massive slags yielded overlapping temperature ranges of 880−1090 °C and 860−1140 °C, respectively. The flat slags point to higher temperatures, falling in the range 1020−1415 °C. Since the expected uncertainty of the geothermometric estimates is not reported in Sack and Ghiorso (1991), the above absolute temperatures may not be very accurate, but should still be robust in relative terms. The presence of accessory cristobalite (identified by XRPD) in coarse slags is a proxy of high temperature conditions, however it cannot be used as geothermometer since it can occur metastably at much lower temperatures (> 900 °C; Mollah et al. 1999; Wahl et al., 1961) than ~~that~~ those predicted by thermodynamic models in a pure SiO_2 system ($T \geq 1470$ °C).

3.5. Radiocarbon dating

Charcoal fragments showed different degrees of carbonization and most of them were mineralized, i.e., impregnated and partly replaced, by Fe-oxyhydroxides and carbonates. Mineralization was a major hindrance for dating, because very mineralized charcoal fragments yielded not sufficient carbon quantities after acid-alkali-acid pretreatment. One exploratory analysis was made in 2006 on a coarse slag found on the surface of the reworked deposit (sample MO304 B) and yielded an age of 2120 ± 30 BP (before present, assumed as 1950 CE ± 1σ), calibrated to 200-100 BCE (Fig. 9a). The mineralization issue was particularly severe for the slags in the buried deposit. For this deposit we could date only one composite sample made of the two subsamples FE-G12-C and FE-G12-D, which gave a virtually identical age of 2103 ± 35 BP, calibrated to 180-50 BCE (Fig. 9b).

286 4. DISCUSSION

287

288 4.1. The copper metallurgical process at Misérègne

289 4.1.1. The furnace charge

290 The Misérègne slags are clearly related to copper production, since we found evidence that
291 chalcopyrite was used in the furnace charge (relicts in coarse slags) and a Cu-Fe-sulfide phase, i.e.,
292 the matte, was produced and processed. This is not surprising, given the occurrence of chalcopyrite-
293 rich copper mines within a few km of the site, such as the Lovignanaz mine along the Clavalité Valley
294 and the Servette mine in the Saint-Marcel Valley (pyrite-chalcopyrite ore hosted in chlorite schists,
295 talc schists and glaucophanites; Castello, 1981; Tumiati et al., 2005; Fig. 2). In particular, matte
296 morphology (i.e., round patches or droplets), texture and composition suggest that the matte was
297 completely molten during the process and indicate different degrees of Cu-enrichment and
298 desulfurization. Starting from a charge of chalcopyrite with variable proportions of pyrite (consistent
299 with the mineralogy of local sulfide orebodies; Castello et al., 1981), the assemblages *iss* + Po_{ss} and
300 Bn_{ss} + Po_{ss}, which are observed in the coarse and massive slags, would form upon cooling below
301 ~1000 °C of a molten sulfide phase (Barton and Skinner, 1979; Yund and Kullerud, 1966). This sulfide
302 phase would be variably desulfurized and Fe-depleted with respect to the starting material (~38 wt%
303 S in pyrrhotite vs. ~53 wt% S in pyrite; ~30 wt% Fe and ~35 wt% S in chalcopyrite and *iss* vs. ~11
304 wt% Fe and ~26 wt% S in bornite), with Bn_{ss} + Po_{ss} representing a slightly more "mature" matte. All
305 the slags are SiO_2-rich (> 25 wt%) and have high Al_2O_3 (9−13 wt%), MgO (4−8 wt%) and TiO_2 (1−2
306 wt %) contents. In particular, the Al_2O_3:MgO:TiO_2 ratios in the coarse (~7:3:1), massive (~7−8:3-4:1)
307 and flat slags (~9:4−5:1) are very close to those in chlorite schists, talc schists and glaucophanites
308 from the same area (~7:4:1 in chlorite schists; ~7:5:1 in talc schists, ~9:6:1 in glaucophanites; Martin
309 et al., 2008), which are the typical host-rocks of sulfide ores in Valle d'Aosta copper deposits (Castello
310 et al., 1981). This suggests the presence of high proportions of gangue minerals in the furnace charge,
311 such as talc (SiO_2 and MgO-rich) and quartz (both observed as relict phases in all the slag types),

312 chlorite-group minerals, (Al_2O_3 and MgO-rich), ilmenite or rutile (TiO_2-rich). Using such an "impure"
313 ore is advantageous because quartz and talc would provide the necessary SiO_2 for producing the slag.
314 Moreover, the addition of Al_2O_3, contained in other gangue minerals, to a binary FeO-SiO_2 system
315 lowers the melting point of the silicate slag by ~100 °C (see the ternary diagram in Fig. 8), resulting
316 both in an earlier onset of the slagging process and in saving of fuel. The nearly eutectic composition
317 of the coarse and massive slags suggests that a well-balanced mix of reactants was used in order to
318 maximize melting. Moreover, the concurrent addition of MgO and TiO_2 (and, to a lesser extent, CaO)
319 would increase the slag fluidity by decreasing the degree of polymerization of the melt (e.g., Best,
320 2002), thus favoring matte settling and separation from the silicate slag.
321
322 4.1.2. Furnace temperatures
323 The comparison between the compositions of the slags and those of experimental melts in the
324 simplified SiO_2-Al_2O_3-FeO system (Fig. 8) suggests melting temperatures ~1080 °C for the coarse
325 and massive slags and 1200−1250 °C for the flat slags. Temperature estimates based on olivine-spinel
326 geothermometry show relatively large variability, even when olivine-hercynite pairs from the same
327 slag sample are considered (Table 2). The interpretation of these estimates is not straightforward,
328 because olivine-hercynite pairs may have formed at any stage of the thermal history of the slag (initial
329 heating, steady-temperature stage and cooling) and could re-equilibrate upon cooling of the system
330 due to subsolidus Mg-Fe interdiffusion (e.g., Ozawa, 1984). Concerning the latter issue, although
331 olivine crystals are strongly zoned from Mg-rich cores to Fe-rich rims, they show no chemical zoning
332 around the hercynite inclusions, suggesting that subsolidus Fe-Mg diffusion was not significant.
333 Therefore, within-sample heterogeneity of geothermometric estimates suggests that the olivine-
334 hercynite pairs were formed over a range of temperatures. Statistically, the highest estimates should
335 be the closest to, and thus represent minimum estimates of, the actual furnace working temperatures.
336 The maximum temperature estimates obtained for the different slag types (~1100 °C for the coarse
337 and massive slags and ~1400 °C for the flat slags) are reasonable and comparable to those estimated

with different methods by other authors for furnace working conditions in prehistoric to Roman sites (1100−1400 °C; e.g., Pelton et al., 2015; Addis et al., 2016).

4.1.3. A multiple step process?

Considering the similar bulk and matte compositions and calculated temperatures, the coarse and massive slags seem to be genetically related. This points to a common smelting process, in which raw high-Fe-S sulfide ore (chalcopyrite + pyrite) was processed to obtain a matte enriched in Cu. However, the massive and coarse slags show important differences concerning the degree of porosity (higher in the coarse slags), the proportion of charcoal and unreacted material (higher in the coarse slags), and olivine morphology. In particular, olivine morphology provides information about the cooling path of the slags (Addis et al., 2016; Donaldson, 1976 and Faure et al., 2003, 2007): in the massive slags, olivine crystals are polyhedral or skeletal, indicating a low degree of undercooling (ΔT, defined as the difference between the temperature of the system liquidus and its actual temperature; Vernon, 2004), which can be related to a steady-state crystallization followed by slow cooling (Faure et al., 2003); in the coarse slags olivine is skeletal or dendritic, which indicates larger ΔT and faster cooling rates. The coarse slags do not show flow structures and their high porosity suggests a higher viscosity compared to the massive slags. Therefore, although they cooled relatively quickly, they are unlikely to have been tapped from the furnace. One interpretation is that the coarse and massive slags were parts of the same slag contained in the furnace: the former were in contact with the air, cooled more rapidly, trapped ascending gas bubbles and included charcoal fragments that floated on the surface; the latter cooled more slowly thanks to the insulating cap provided by the upper coarse layer. An alternative hypothesis is that the massive slags were allowed to cool slowly in a relatively well-insulated furnace (with the purpose of allowing the matte contained in the slag to settle); an earlier interruption of the same process would have resulted in a partially reacted coarse slag (thus explaining their higher proportion of unreacted material), which rapidly cooled when the furnace was torn down or raked off.

Compared to the massive and coarse slags, the flat slags are more Fe-rich and Cu-poor and contain more Cu-rich matte droplets. Moreover, olivine morphology indicates an initial low ΔT (polyhedral crystals) followed by a high ΔT stage, i.e., quenching (dendritic crystals). This observation, together with the presence of flow structures, is compatible with slag tapping. Most likely, considering the different matte and slag compositions, the flat slags are not a mere evolution of the other two slag types, but rather the product of a distinct smelting process, in which the matte obtained from the first smelting was re-processed to obtain metallic copper. Before the second smelting, the matte was probably roasted in air (Tylecote, 1992), i.e., oxidized to remove most of the sulfur as SO_2; the oxidation, however, was incomplete, since some matte is still found in the flat slags. Since the flat slags have similar Al_2O_3 and TiO_2 contents to the other slag types, we suppose that a certain amount of local rocks or earlier-stage slags was deliberately added to the charge as a flux for the second smelting. The more Fe-rich composition of the resulting charge may have required higher temperatures to achieve efficient melting (Fig. 8). The small average size of Misérègne coarse and massive slags and their common angular shape may be related with matte/copper recovery by crushing of the products of the first smelting.

4.1.4. Mining industry and copper metallurgy in the Valle d'Aosta during the Iron Age

Our dating constrains the metallurgical activity at the Misérègne site to the II-I century BCE. To the best of our knowledge, this is the earliest archeometric evidence of copper metallurgy in the north-western Italian Alps. Historical sources report that in the Iron Age the Salassi, a Celtic tribe settled in an area roughly comprising the Valle d'Aosta and Canavese (a subalpine region the south-southeast of the Valle d'Aosta), were renowned for extracting copper, silver and especially gold (Strabo, *Geographia*, book IV, chapter 6, 7; Artom, 1935; Oberziner, 1900; Pipino, 2003; Brecciaroli and Taborelli, 2011). In particular, the Salassi exploited gold placers, located in the Ivrea morainic amphitheater at the mouth of the Valle d'Aosta (Pipino, 2003; Brecciaroli and Taborelli, 2011), by diverting the Dora and Elvo river and using much of the water to wash the sediments, thus damaging

389 the downstream agricultural activities (Strabo, *Geographia*, IV, 6.7; Dio Cassius, *Historia romana*,
390 fragment 245). The control of the water and of the mines and, in particular, the frequent raids that the
391 Salassi made in the adjacent territories, were the pretext for the Romans to wage war on the Salassi
392 (Artom, 1935). After a first defeat in 143 BCE, around 140 BCE the Romans seized the gold mines
393 ("aurifodinae") (Pipino, 2003; Brecciaroli and Taborelli, 2011) and in 100 BCE they conquered the
394 region enclosed in Ivrea morainic amphitheater and founded the Eporedia (Ivrea town) colony (Bocca
395 and Centini, 2005). However, in the I century BCE the Romans, which recognized the strategic
396 position of the Valle d'Aosta as a gateway to the central Gaul (through the Little and Great St Bernard
397 passes), repeatedly attacked the Salassi, until they definitively imposed their rule on the region by
398 founding the military colony of *Augusta Praetoria* (Aosta town) in 25 BCE (Strabo, Geographia, IV,
399 6.7; Suetonius, De Vita Caesarum, Augustus, chapter XXI; Gruen, 2006). From the above
400 documentation, it is uncertain whether copper production at Misérègne was carried out by the Salassi
401 or if it was promoted by the arrival of Roman entrepreneurs. We are not aware of any historical source
402 specifically referring to Iron Age copper mining and metallurgy in Valle d'Aosta region, if we exclude
403 the information reported by Pliny the Elder in his *Naturalis Historia* (book XXXIV, chapter 2) about
404 a good quality of copper coming for a short period from the territories of the Ceutrones, i.e., the region
405 of Tarentaise (France; Hirt, 2010), adjoining the Valle d'Aosta to the west. The mining/metallurgical
406 sites may have been overlooked by the Romans because of their "local" character or because they had
407 already been abandoned by the I century CE; also, their importance may have been obscured by the
408 much more productive ore deposits in Gaul and Spain (Nicolet, 2006). This notwithstanding, traces
409 of Roman structures rising on a slag deposit near the Servette copper mine (Framarin, 2011), located
410 6 km south-east of Misérègne (Fig. 2), would confirm the presence of early metallurgical activities
411 shortly prior to or during the Roman domination.
412
413 5. Conclusions
414

In this paper, we present the first direct evidence of early copper smelting in Valle d'Aosta region. At the Misérègne metallurgical site, an impure chalcopyrite + pyrite ore, compatible with that occurring in nearby mines, was smelted to produce copper and different types of slags. Coarse and massive slags have similar compositions and sulfide associations. Their origin could be interpreted in two different ways: (i) the two slag types were sitting at different levels within the furnace (the coarse slags were the upper viscous portion that entrapped gas bubbles and less dense charcoal/wood, quartz and talc fragments; the massive slags represented the molten slag that accumulated on the bottom of the furnace); (ii) the massive slags are the end product of first smelting (they were allowed to cool slowly in the furnace, probably to let the matte settle through the slag), while coarse slag represent the outcome of an earlier and sudden interruption of the same process (possibly obtained by demolishing the furnace). The flat slags show substantially different morphologies and chemical compositions, suggesting that these slags were tapped during a separate and more advanced smelting process. Minimum furnace working temperatures estimated by olivine-spinel geothermometry are consistent with a multiple-step smelting process, involving a lower-temperature stage that produced the coarse and massive slags, close to the eutectic conditions, and a subsequent higher-temperature (≥~1400 °C) stage that produced the flat slags.

Our radiometric data constrain the metallurgical activity to the II-I century BCE, i.e., shortly prior to or during the Roman domination of the Valle d'Aosta, and to our knowledge are the first direct archeometric evidence of copper-making in Valle d'Aosta region and in the north-western Italian Alps.

ACKNOWLEDGMENTS

We would like to thank Andrea Risplendente (Earth Sciences Department, University of Milan) for the technical assistance during the EPMA analyses and Dr. Federico Zorzi (Geosciences Department, University of Padua) for performing XRPD analyses. We are also grateful to Prof. Franco Gianotti (University of Turin) and Dr. Sandro Rossato (University of Padua) for their help in

441 the analysis and interpretation of geomorphological data. LT and SM acknowledge financial
442 resources made available by the project between the University of Padua and Fénis municipality,
443 named “Convenzione per la realizzazione dello studio dei siti minerari della Val Ponton, Val
444 Clavalité e di Fenis (Aosta)”. PN acknowledges financial support by Progetto di Ateneo 2013
445 CPDA138741 ‘‘Copper metallogenesis and provenancing in the Alpine realm” (University of
446 Padua).

447

448 APPENDIX

449 The procedure used for FeO determination is based on a modified version of the method described
450 by Pratt (1984): a known quantity of sample, previously is prepared into powder, is mixed in a Pt
451 crucible with 15 ml of an acidic mixture composed of one part of deionized H_2O, one part of
452 hydrofluoric acid (HF 40%) and one part of sulfuric acid (H_2SO_4 95%). The crucible is then placed
453 on a preheated (180 °C) graphite plate for ca. 8 minutes. The content of the crucible is then poured
454 into a polyethylene beaker containing 300 ml of deionized H_2O, 5 ml of H_2SO_4 and 0.6 g of H_3BO_3,
455 and stirred. Titration is performed using a 0.1 N solution of potassium permanganate ($KMnO_4$).
456 During the titration the following reaction occurs:

457 $$2\ KMnO_4 + 10\ FeSO_4 + 8\ H_2SO_4 \rightarrow K_2SO_4 + 2\ MnSO_4 + 8\ H_2O + 5\ Fe_2(SO_4)_3$$

458 The volume (in ml) of permanganate needed for the titration is used to calculate the percentage of
459 FeO in the sample according to this formula:

460 $$\%\ FeO = [\text{used } KMnO_4 \text{ solution (ml)} \cdot 0.007185\ (\text{g/ml}) \cdot 100]/\text{sample weight (g)}$$

461 Where 0.007185 is the quantity (in g) of FeO equivalent to 1 ml of 0.1 N $KMnO_4$ solution.

462

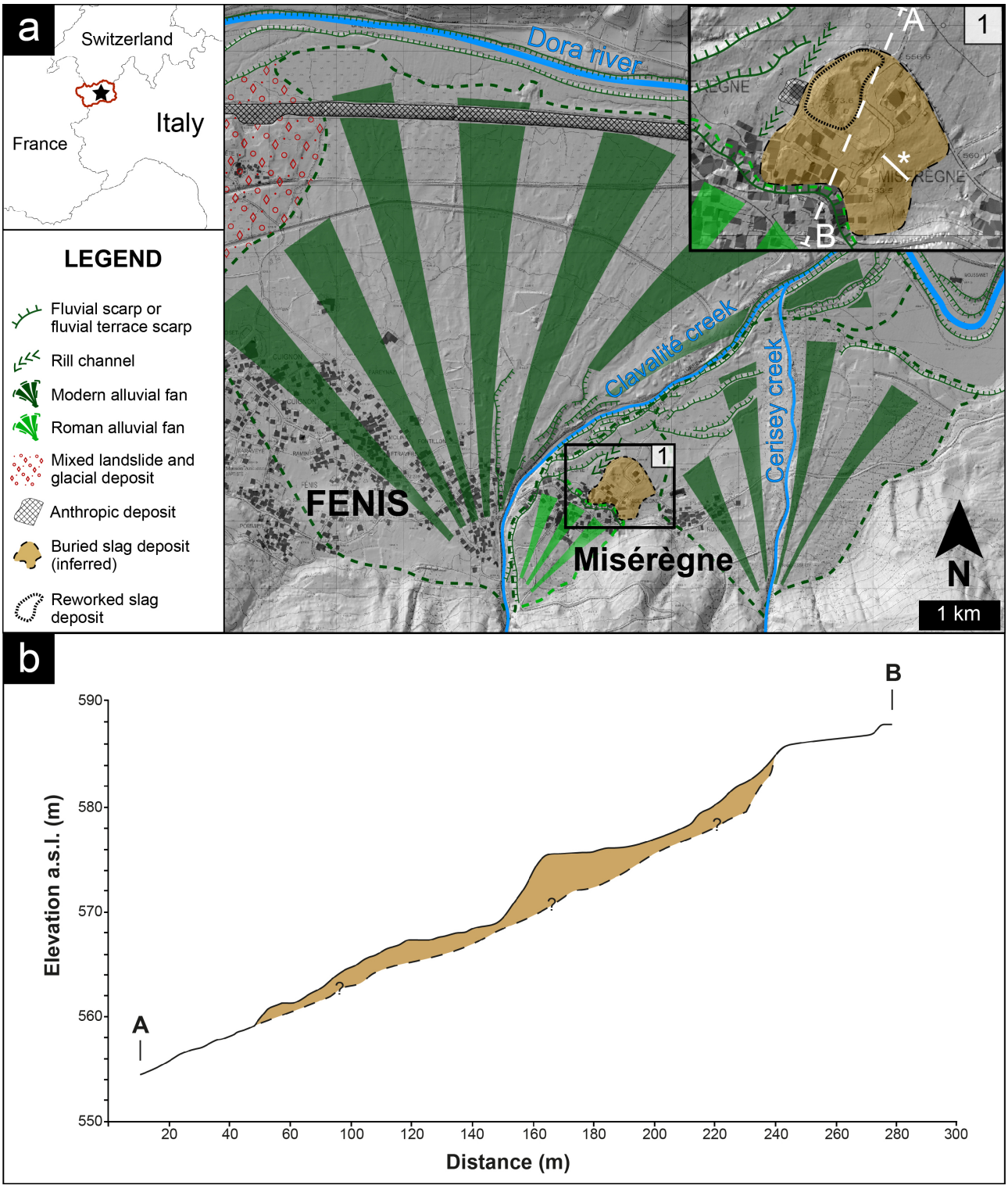

Fig. 1. (a) Simplified geomorphological map of the Fénis area. Valle d'Aosta region is highlighted and the star indicates the studied area. In the inset, the Misérègne slag deposit is outlined and the asterisk indicates the section through the buried slag deposit shown in Fig. 3. (b) Profile through the Misérègne slag deposit as inferred from the digital terrain model. Vertical scale is exaggerated. Cartographic base from the website of Regione Autonoma Valle d'Aosta (http://geonavsct.partout.it/pub/GeoCartoSCT/index.html).

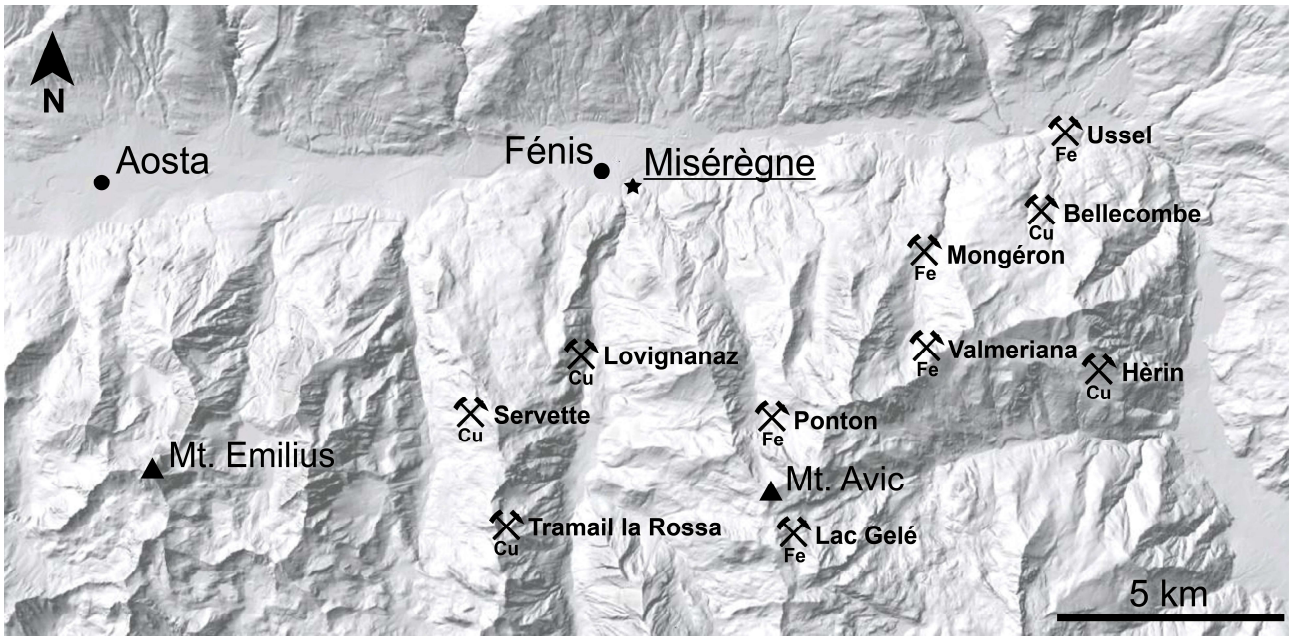

Fig 2. Principal Fe and Cu mines and orebodies in the southern Valle d'Aosta region. Fe: magnetite ore. Cu: pyrite-chalcopyrite ore. Cartographic base from the website of Regione Autonoma Valle d'Aosta (http://geonavsct.partout.it/pub/GeoCartoSCT/index.html).

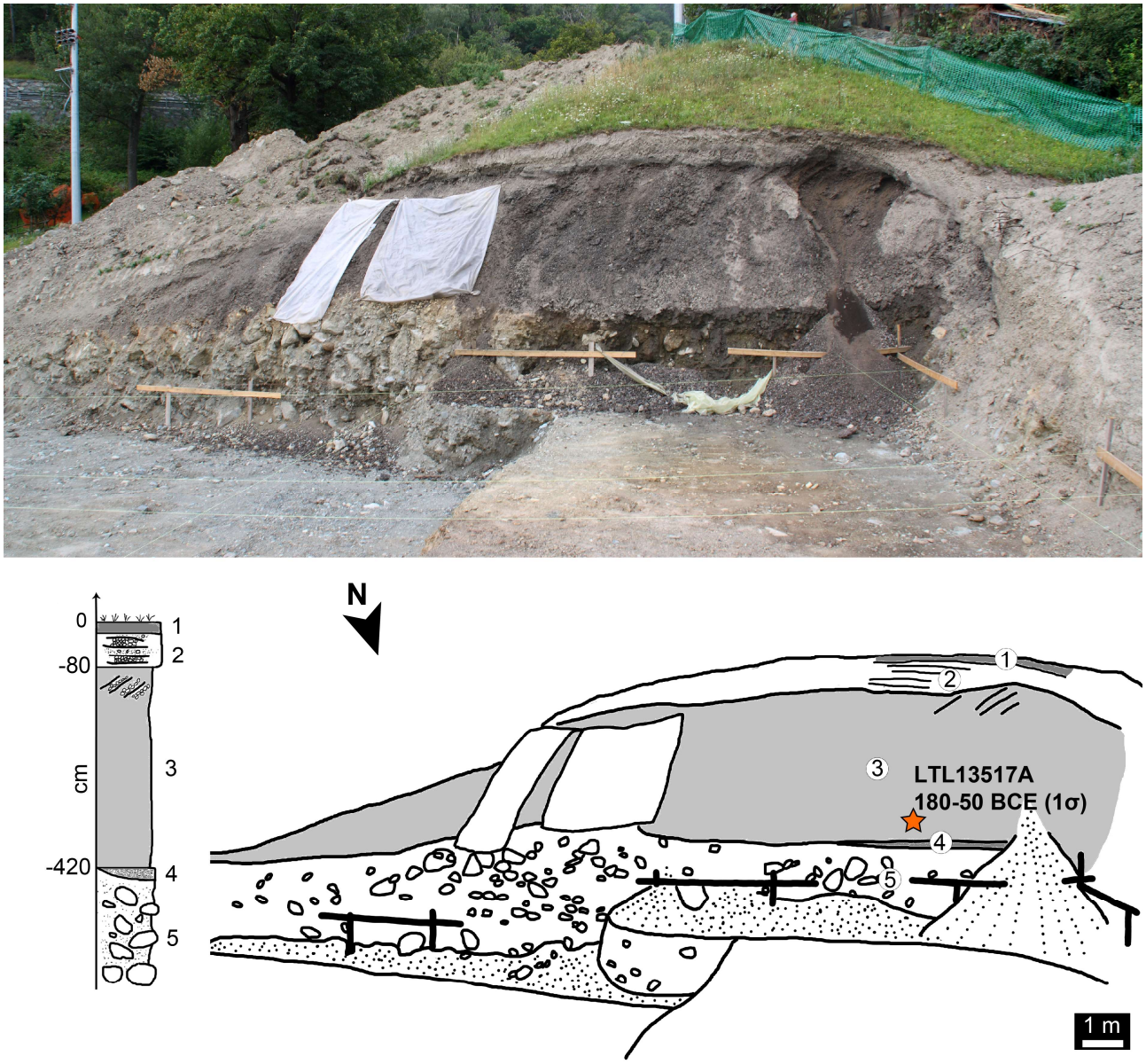

Fig. 3. Section of the Misérègne slag deposit. 1: soil (15-20 cm). 2: slag strata interlayered with sand beds (60 cm). 3: slag deposit, cross-stratified towards the upper surface (340 cm). 4: lenticular sand bed (20 cm). 5: matrix-supported chaotic coarse-grained deposit (sub-angular pebbles, cobbles and boulders) belonging to the alluvial fan of the Clavalité creek. Star indicates the position of the radiocarbon-dated sample.

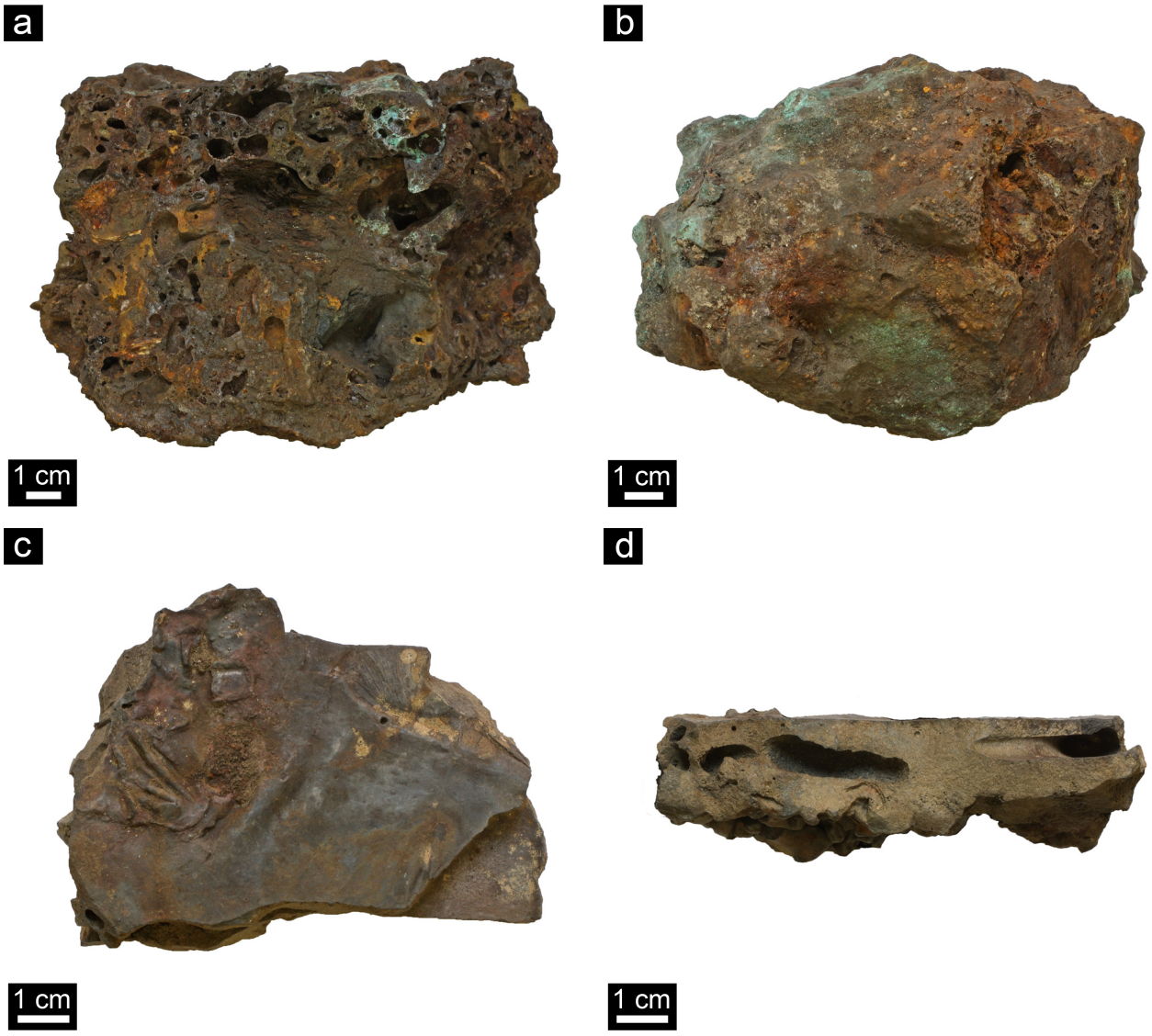

Fig. 4. Representative slag samples from the Misérègne deposit. (a) coarse slag; (b) massive slag; (c) flat slag, plan view; (d) flat slag, profile.

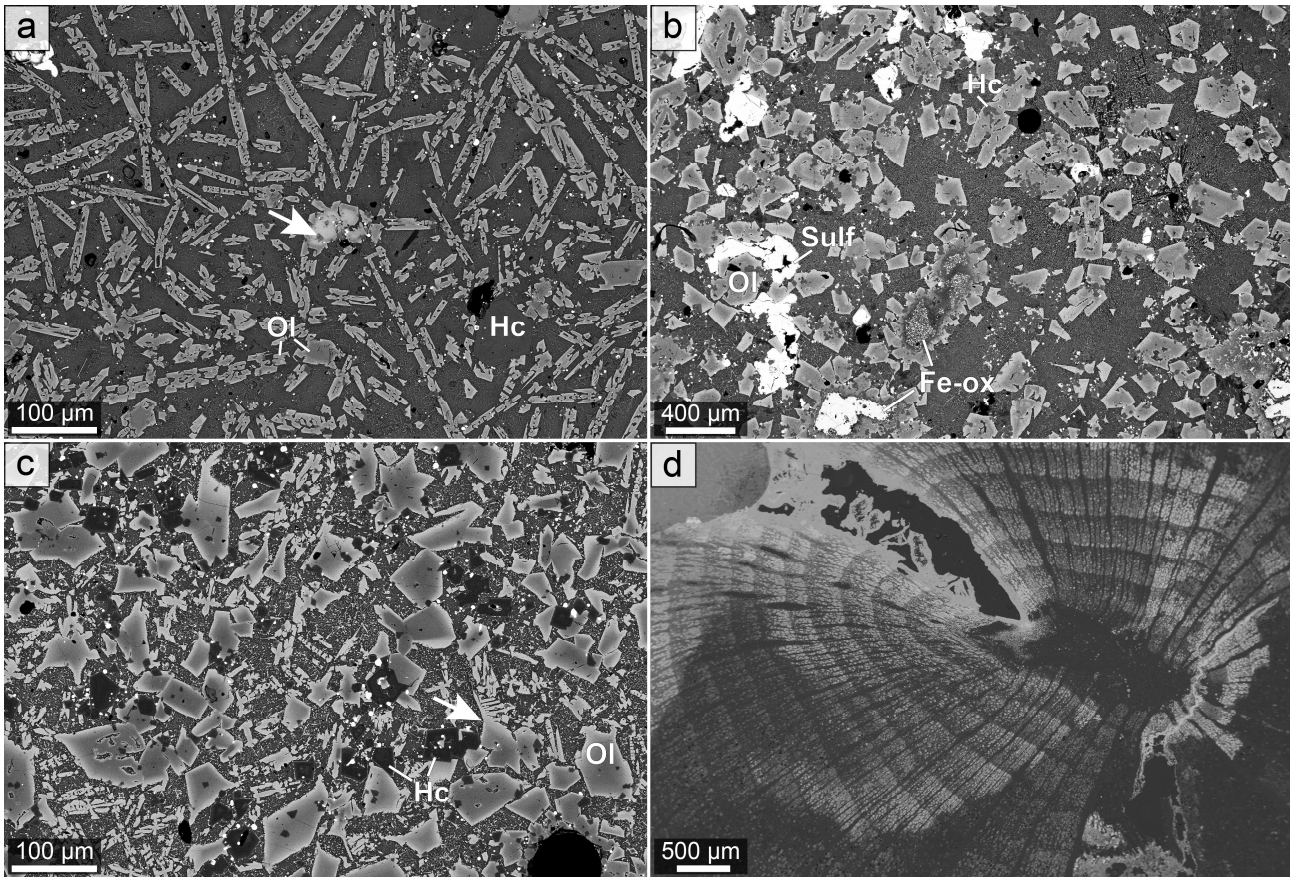

487

488 **Fig. 5.** SEM-BSE images of microstructural features of the Misérègne slags. (a) Coarse slag, with
489 zoned dendritic olivine (Ol) and euhedral hercynite (Hc). Hercynite is also included in olivine
490 (arrow). Tiny white patches disseminated in the slag are sulfides (matte). (b) Massive slag, with zoned
491 polyhedral olivine and hercynite. White patches are sulfides (Sulf) and Fe-oxides (Fe-ox). (c) Flat
492 slag, with zoned polyhedral, dendritic and transitional (arrow) olivine and euhedral hercynite. (d)
493 Radial section of a carbonized branch (*Fagus sylvatica*). Note that the pores are variably impregnated
494 with Fe-oxyhydroxides (light grey portions).

495

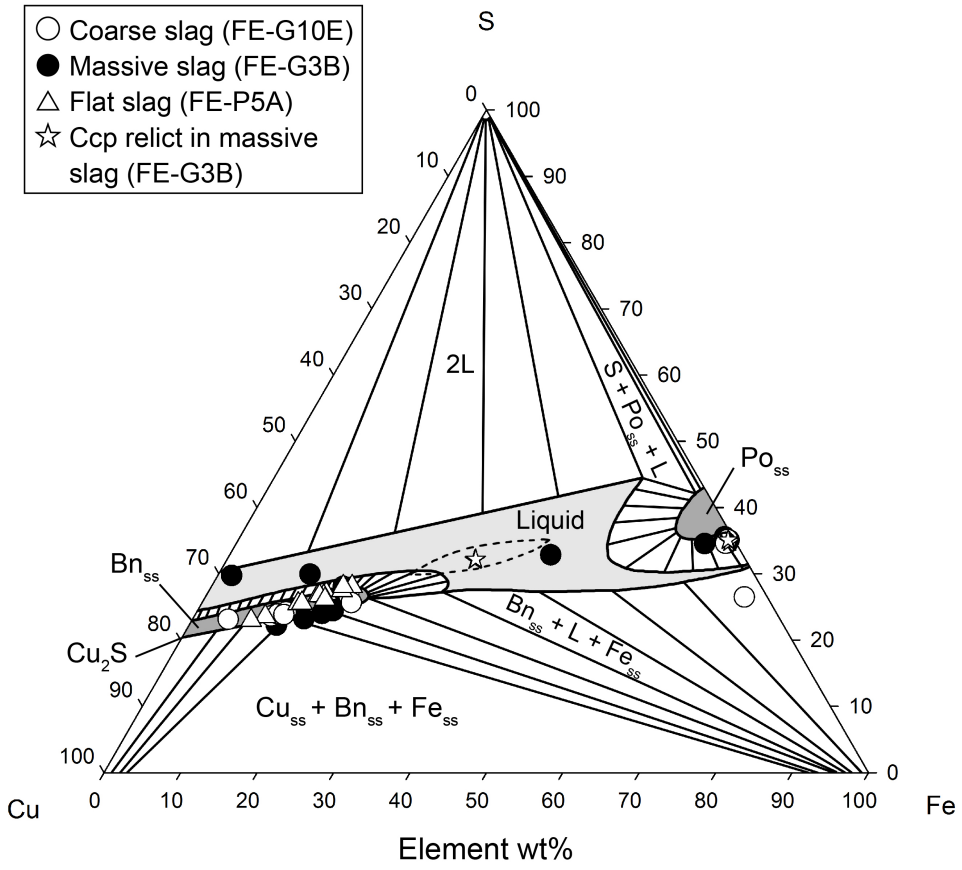

Fig. 6. Sulfide compositions plotted on a Cu-Fe-S phase diagram at 1000°C (modified from Barton and Skinner, 1979). *Iss* is not stable at this temperature and its stability field at 700°C (Yund and Kullerud, 1966) is shown (dashed lines). "Ccp relict" refers to ~~to~~ a fragment of slightly reacted chalcopyrite ore.

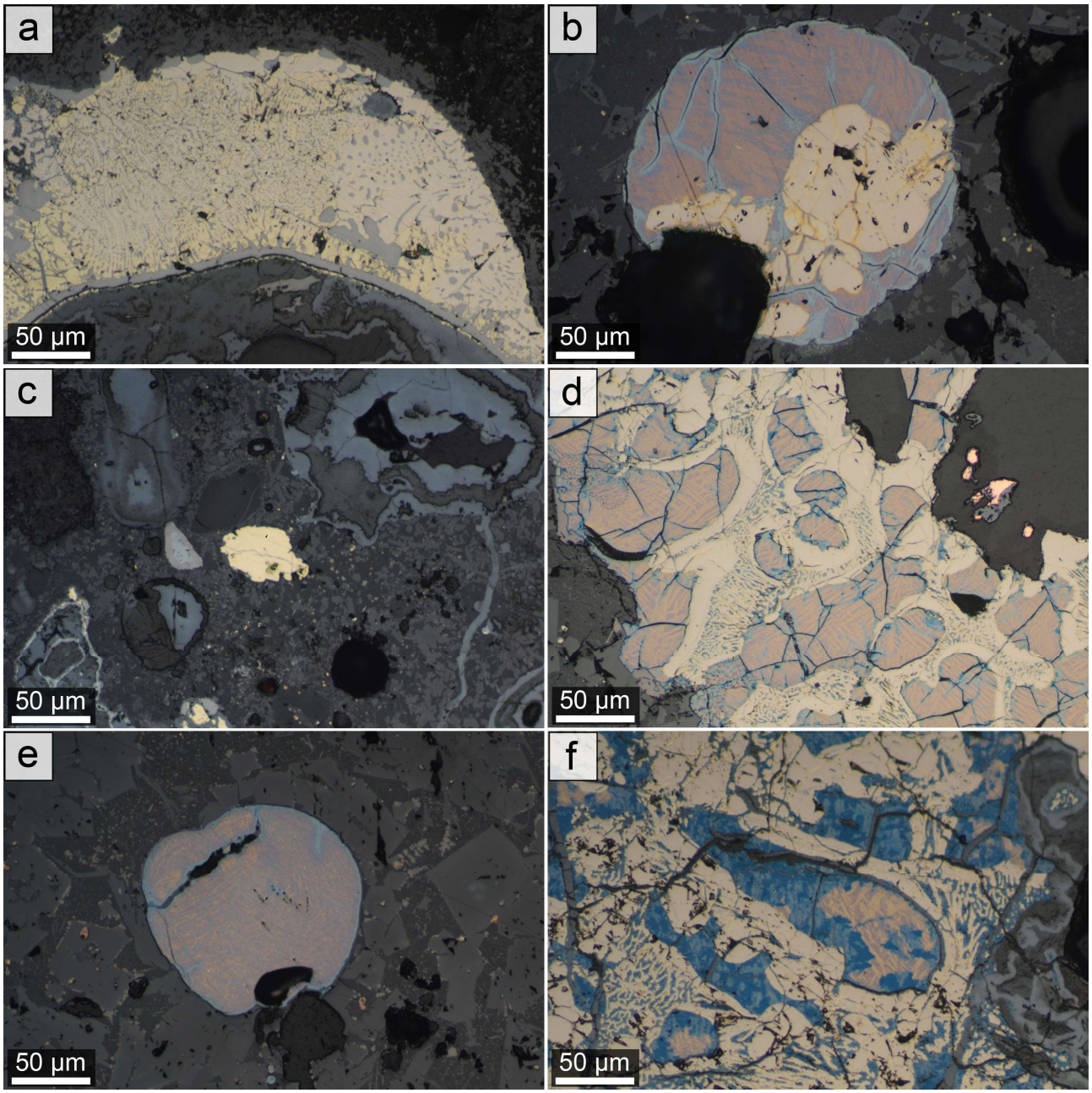

Fig. 7. Microphotographs under reflected polarized light of sulfides in coarse (a, b, c, f), massive (d) and flat (e) slags. (a) Po_{ss} (cream) + *iss* symplectite (yellow); light-grey areas within and around the symplectite are secondary Fe-oxyhydroxides. (b) Droplet composed by Bn_{ss} (purplish brown) and Po_{ss} (cream) associated with very minor *iss* (yellow patches around Po_{ss} grains). (c) Relict chalcopyrite fragment (at the center) (d) Round Bn_{ss} grains (pinkish brown) enveloped by Po_{ss} (cream), with interstitial Bn_{ss}-Po_{ss} symplectite. Dissected curls of metallic copper (bright pink) occur in an empty area. (e) Droplet of Cu-rich Bn_{ss}. (f) Extensive alteration of Bn_{ss} (at the center) into fine-grained covellite (dark blue) + digenite (greyish blue); alteration does not affect Po_{ss} (cream). In all the pictures Bn_{ss} shows exsolution lamellae of Cu-richer Bn_{ss} (more violet). Blue patches, mainly occurring along the fractures and rims of Bn_{ss}, are an alteration to covellite/digenite analogously to what is shown in (f).

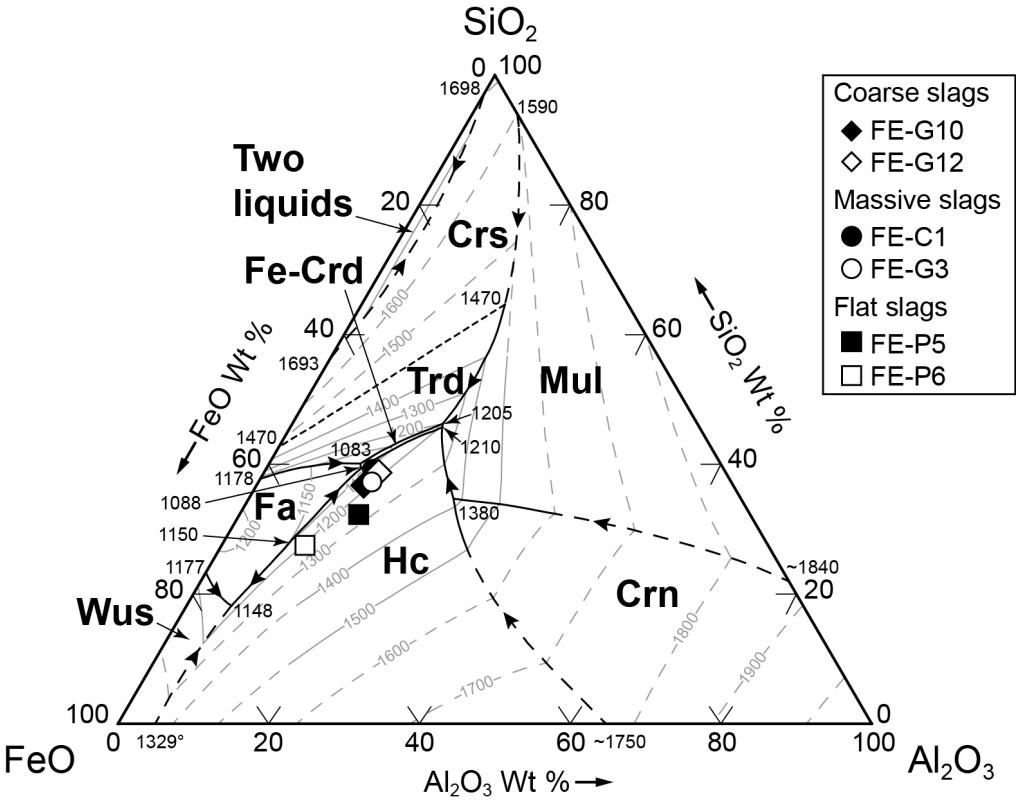

515

516 **Fig. 8.** FeO-Al_2O_3-SiO_2 phase diagram at 1 atm (modified from Levin et al., 1964). Al_2O_3 and FeO
517 were recalculated as recommended by Tumiati et al. (2005): Al_2O_3 = Al_2O_3 + TiO_2 + Cr_2O_3 and FeO
518 = FeO + MgO + MnO + CaO (+ Na_2O + K_2O); all iron is considered to be FeO. Numbers refer to
519 temperatures in °C. Mineral abbreviations: Crs = cristobalite; Crn = corundum; Fa = fayalite; Fe-Crd
520 = Fe-cordierite; Hc = hercynite; Trd = tridymite; Wus = wüstite. All the fields indicated by mineral
521 names are actually divariant surfaces where melt is also present.

522

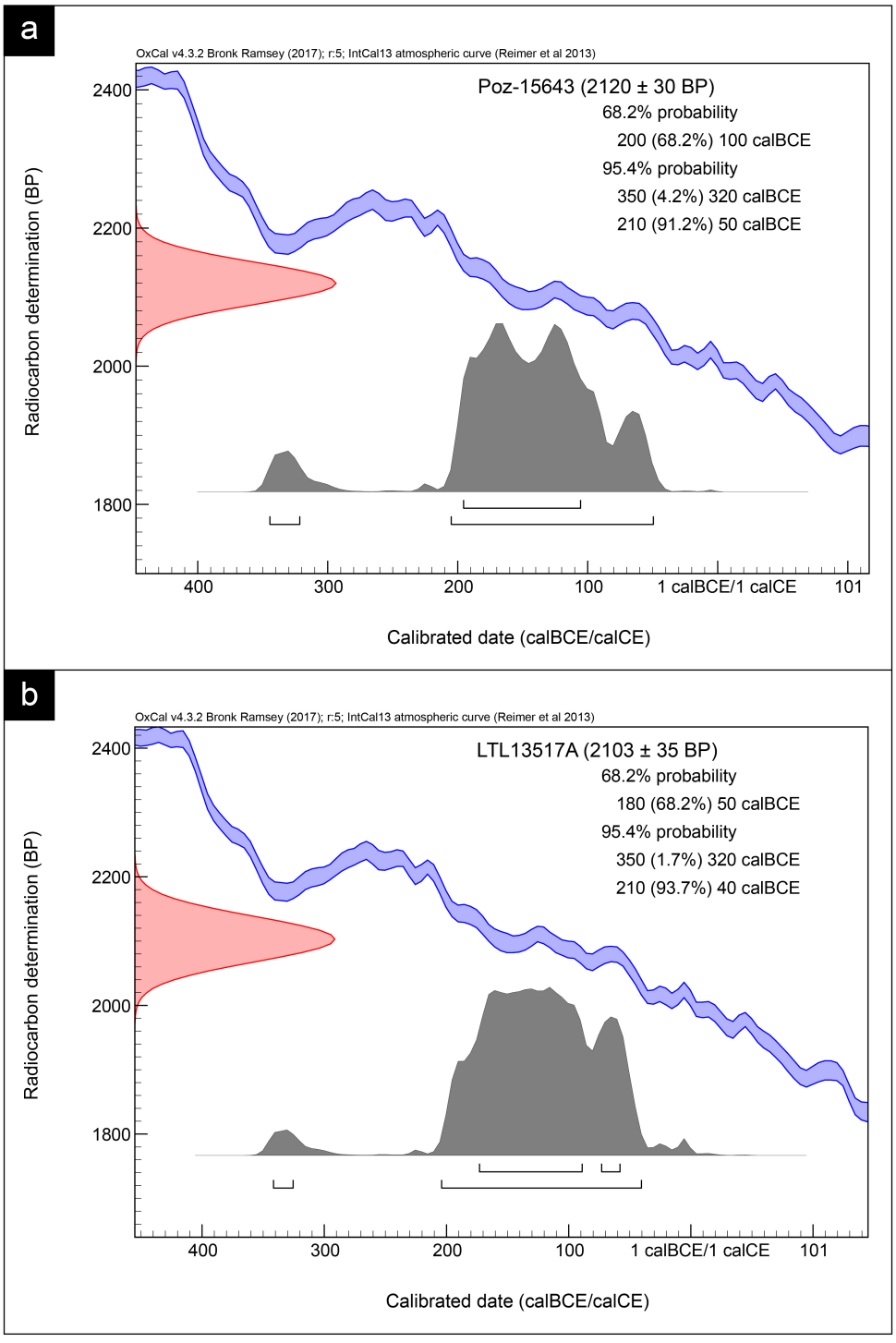

Fig. 9. Radiocarbon dating of samples of: (a) Poz-15643 (= MO304 B) from the reworked deposit; (b) LTL13517A (= FE-G12-C/D) from the buried deposit. Plots have been prepared using OxCal software v4.3.2 (Bronk Ramsey, 2009, 2017).

529 REFERENCES

530 Addis, A., 2013. Late Bronze Age metallurgy in the Italian Eastern Alps: copper smelting slags and
531 mine exploitation, PhD Thesis, Geosciences Department, University of Padua, 222 pp.
532
533 Addis, A., Angelini, I., Nimis, P., Artioli, G., 2016. Late Bronze Age copper smelting slags from
534 Luserna (Trentino, Italy): interpretation of the metallurgical process. Archaeometry 58, 96-114.
535
536 Artom, E., 1935. L'industria dell'oro presso i Salassi. Società industriale grafica Fedetto & c.
537
538 Bachmann, H.G, 1982. The identification of slags from archaeological sites. Institute of Archaeology
539 Occasional Publications, 6, 36 pp.
540
541 Barton, P.B., Skinner, B.J., 1979. Sulfide mineral stabilities. In: Barnes, H.L. (Ed.), Geochemistry of
542 Hydrothermal Ore Deposits. Wiley, pp. 278-403.
543
544 Best, M.G., 2003 Igneous and Metamorphic Petrology, 2nd ed., Blackwell, Berlin, 758 pp.
545
546 Bocca, C., Centini, M., 2005. Sulle tacce dei Salassi. Origine, storia e genocidio di una cultura alpina.
547 Quaderni di cultura alpina. Priuli e Verlucca, 87 pp.
548
549 Brecciaroli Taborelli, L., 2011. Oro, pane e scrittura. Memorie di una comunità "inter Vercellas et
550 Eporediam" Edizioni Quasar, 533 pp.
551
552 Bronk Ramsey, C., 2009. Bayesian analysis of radiocarbon dates. Radiocarbon 51, 337-360.
553
554 Bronk Ramsey, C., 2017. OxCal software (version 4.3.2), https://c14.arch.ox.ac.uk/oxcal.html
555
556 Calcagnile, L., Quarta, G., D'Elia, M., Rizzo, A., Gottdang, A., Klein, M., Mous, D. J. W., 2004. A
557 new accelerator mass spectrometry facility in Lecce, Italy. Nucl. Instrum. Meth. B 223, 16-20.
558
559 Castello, P., 1981. Inventario delle mineralizzazioni a magnetite, ferro-rame e manganese del
560 complesso piemontese dei calcescisti con pietre verdi in Valle d'Aosta. Ofioliti 6, 5-46.
561

562 D'Elia, M., Calcagnile, L., Quarta, G., Sanapo, C., Laudisa, M., Toma, U., Rizzo, A., 2004. Sample
563 preparation and blank values at the AMS radiocarbon facility of the University of Lecce. Nucl.
564 Instrum. Meth. B 223, 278-283.
565
566 Di Gangi, G., 1999. L'attività estrattiva e metallurgica nell'arco alpino occidentale tra medioevo ed
567 età moderna. La Valle d'Aosta: note e documenti, Att. Conv. Miniere fucine e metallurgia nel
568 Piemonte medievale e moderno, Rocca de' Baldi (CN), 12 dicembre 1999, 103-123.
569
570 Donaldson, C. H., 1976. An experimental investigation of olivine morphology. Contrib. Mineral. Petr.
571 57, 187-213.
572
573 Faure, F., Trolliard, G., Nicollet, C., Montel, J. M., 2003. A developmental model of olivine
574 morphology as a function of the cooling rate and the degree of undercooling. Contrib. Mineral. Petr.
575 145, 251-263.
576
577 Faure, F., Schiano, P., Trolliard, G., Nicollet, C., Soulestin, B., 2007. Textural evolution of polyhedral
578 olivine experiencing rapid cooling rates. Contrib. Mineral. Petr. 153, 405-416.
579
580 Gerbore, E.E., 2000. Miniere e forni di fusione, in: Fénis. Une communauté au fil de l'histoire.
581 Musumeci Editore, pp. 287-299.
582
583 Gruen, E.S., 2006. The expansion of the empire under Augustus. In: Bowman, A.K., Champlin, E.,
584 Lintott, A. (Eds.) The Cambridge ancient history, 2nd edition, Vol. X, The Augustan Empire, 43 B.C-
585 A.D. 69. Cambridge University Press, pp. 147-196.
586
587 Govindaraju, K., 1994. Compilation of working values and sample description for 383 geostandards.
588 Geostandard Newslett. 18, 1-158.
589
590 Hirt, A.M., 2010. Imperial mines and quarries in the Roman world: organizational aspects 27 BC-AD
591 235. Oxford University Press, 551 pp.
592
593 Irvine, T.N., 1965. Chromian spinel as a petrogenetic indicator: Part 1. Theory. Can. J. Earth. Sci. 2,
594 648-672.
595

596 Levin, E.M., Robbins, C.R., McMurdie, H.F., 1964. Phase diagrams for ceramists. The American
597 Ceramic Society Inc., Columbus, Ohio, 601 pp.
598
599 Martin, S., Godard, G., Rebay, G., 2004. Walking on a palaeo ocean floor. The subducted Tethys in
600 the Western Alps-An excursion guide. J. Virtual Explorer 16, 1-46.
601
602 Mollah, M.Y.A., Promreuk, S., Schennach, R., Cocke, D.L., Güler, R., 1999. Cristobalite formation
603 from thermal treatment of Texas lignite fly ash. Fuel 78, 1277-1282.
604
605 Nicco, R., 1987. L'industrializzazione in Val d'Aosta - Studi e documenti, Quaderni dell'Istituto
606 Storico della Resistenza in Valle d'Aosta, I, II, III, 89 pp.
607
608 Nicolet, C., 2006. Economy and society, 133-43 B.C. In: Crook, J. A., Lintott, A., Rawson, E. (Eds.),
609 The Cambridge ancient history, 2nd edition, Vol. IX, The Last Age of the Roman Republic, 146-43
610 B.C. Cambridge University Press, pp. 599-643.
611
612 Oberziner, G., 1900. Le guerre di Augusto contro i popoli alpine. Loescher, Rome, 239 pp.
613
614 Ozawa, K., 1984. Olivine-spinel geospeedometry: analysis of diffusion-controlled Mg-Fe^{2+} exchange.
615 Geochim. Cosmochim. Ac. 48, 2597-2611.
616
617 Pipino, G., 2003. Oro, Miniere, Storia. Miscellanea di giacimentologia e storia mineraria italiana.
618 Museo Storico Oro Italiano, 510 pp.
619
620 Pratt, J.H., 1984. On the determination of ferrous iron in silicates. Am. J. Sci., 284, 149-151.
621
622 Reimer, P.J., Bard E., Bayliss, A., Beck, J.W., Blackwell, P.G., Bronk Ramsey, C., Buck, C.E.,
623 Cheng, H., Edwards, R.L., Friedrich, M., Grootes, P.M., Guilderson, T.P., Haflidason, H., Hajdas,
624 I., Hatté, C., Heaton, T.J., Hoffmann, D.L., Hogg, A.G., Hughen, K.A., Kaiser, K.F., Kromer, B.,
625 Manning, S.W., Niu, M., Reimer, R.W., Richards, D.A., Scott, E.M., Southon, J.R., Staff, R.A.,
626 Turney, C.S.M, van der Plicht, J., 2013. IntCal13 and Marine13 radiocarbon age calibration curves
627 0–50,000 years cal BP. Radiocarbon 55, 1869-1887.

Rietveld, H., 1969. A profile refinement method for nuclear and magnetic structures. J. Appl. Crystallogr. 2, 65–71.

Robilant (Nicolis de), E.-B., 1786. Essai géographique suivi d'une topographie souterraine, minéralogique & d'une docimasie des Etats de S. M. [Sa Majesté] en terre ferme, Mémoires de l'Académie royale des Sciences, Turin, I, 191-304.

Robilant (Nicolis de), E.-B, 1788. Description particulière du Duché d'Aoste, suivie d'un essai sur deux minières des Anciens Romains et d'un supplément à la théorie des montagnes et des mines, Mémoires de l'Académie royale des Sciences, Turin, III, 254-274 + pl. vii-ix.

Sack, R.O., Ghiorso, M.S., 1991. Chromian spinels as petrogenetic indicators: thermodynamics and petrological applications. Am. Mineral. 76, 827-847.

Sáez, R., Nocete, F., Nieto, J. M., Capitán, M.Á., Rovira, S., 2003. The extractive metallurgy of copper from Cabezo Juré, Huelva, Spain: chemical and mineralogical study of slags dated to the third millenium BC. Can. Mineral. 41, 627-638.

Tumiati, S., Casartelli, P., Mambretti, A., Martin, S., 2005. The ancient mine of Servette (Saint-Marcel, Val d'Aosta, Western Italian Alps): a mineralogical, metallurgical and charcoal analysis of furnace slags, Archaeometry 47, 317-340.

Tylecote, R.F., 1992. A history of metallurgy, 2nd edition. Institute of Materials, London, 205 pp.

Vaughan, D.J., (Ed.), 2006. Sulfide mineralogy and geochemistry (Vol. 61). Mineralogical Society of America, 714 pp.

Vernon, R.H., 2004. A practical guide to rock microstructure. Cambridge University Press, 606 pp.

Wahl, F.M., Grim, R.E., Graf, R.B. 1961. Phase transformations in silica as examined by continuous X-ray diffraction. Am. Mineral. 46, 196-208.

661 Yund, A.R., Kullerud, G., 1966. Thermal stability of assemblages in the Cu-Fe-S system, J. Petrol. 7,
662 454-488.